Top Laminated Graphene Electrode in a Semitransparent Polymer Solar Cell by Simultaneous Thermal Annealing/Releasing Method

Yu-Ying Lee,[†] Kun-Hua Tu,[†] Chen-Chieh Yu,[†] Shao-Sian Li,[†] Jeong-Yuan Hwang,[‡] Chih-Cheng Lin,[†] Kuei-Hsien Chen,[§] Li-Chyong Chen,[‡] Hsuen-Li Chen,[†] and Chun-Wei Chen[†,*]

[†]Materials Science and Engineering, National Taiwan University, Taipei, 106 Taiwan, [‡]Center for Condensed Matter Sciences, National Taiwan University, Taipei, 116, Taiwan, and [§]Institute of Atomic and Molecular Sciences, Academic Sinica, Taipei, 10617, Taiwan

ABSTRACT In this article, we demonstrate a semitransparent inverted-type polymer solar cell using a top laminated graphene electrode without damaging the underlying organic photoactive layer. The lamination process involves the simultaneous thermal releasing deposition of the graphene top electrode during thermal annealing of the photoactive layer. The resulting semitransparent polymer solar cell exhibits a promising power conversion efficiency of approximately 76% of that of the standard opaque device using an Ag metal electrode. The asymmetric photovoltaic performances of the semitransparent solar cell while illuminated from two respective sides were further analyzed using optical simulation and photocarrier recombination measurement. The devices consisting of the top laminated transparent graphene electrode enable the feasible roll-to-roll manufacturing of low-cost semitransparent polymer solar cells and can be utilized in new applications such as power-generated windows or multijunction or bifacial photovoltaic devices.

KEYWORDS: graphene electrode · top lamination · semitransparent solar cell · polymer solar cell · roll-to-roll

Polymer solar cells have attracted considerable interest for fabricating low-cost, large-area, and mechanically flexible photovoltaic devices,[1−3] though the efficiency is still low compared to that of conventional inorganic counterparts. Another inherent advantage of polymer solar cells is the possibility to realize semitransparent photovoltaic device structures, which can be utilized in novel applications such as power-generated windows for buildings and automobiles[4] and multijunction solar cells formed by stacking two or more devices with different spectral responses.[5] Several semitransparent organic photovoltaic devices have been demonstrated using various types of transparent electrodes, such as indium tin oxide (ITO),[6] conducting polymer,[7] and nanowire meshes[8] on top of the photoactive layers. Graphene, which consists of a single-atom-thick plane of carbon atoms arranged in a honeycomb lattice, has demonstrated excellent carrier transport arising from a unique two-dimensional (2D) energy dispersion.[9] In addition, graphene also exhibits a high transparency, with a transmittance of 97.6% from single-layer graphene,[10] making it a promising candidate for transparent electrode applications. One critical issue in the fabrication of semitransparent organic solar cells is that the electrode must be deposited on top of the cell without damaging the underlying organic photoactive layer to establish a good electrode contact. Although several studies have reported on the graphene-based electrode for replacing the ITO bottom electrode in organic photovoltaic devices,[11−13] until now, the use of the graphene top electrode in organic photovoltaics is still very limited. In this article, we demonstrate a simple lamination process for depositing the graphene electrode on top of a polymer photovoltaic device, resulting in a semitransparent polymer solar cell with a power conversion efficiency of over 75% of that of the standard opaque device using an Ag metal electrode. The lamination process involves the simultaneous thermal releasing deposition of the graphene top electrode during thermal annealing of the photoactive layers and can be fully integrated with the roll-to-roll fabrication procedures of polymer solar cells.

The conventional polymer solar cells usually consist of a device structure of ITO/PEDOT:PSS/photoactive layer/Al. Promising power-conversion efficiencies (PCEs) of 4−5% have been achieved using a blend consisting of a poly(3-hexylthiophene) (P3HT) and a fullerene derivative, [6,6]-phenyl-C61-butyric acid methyl ester (PCBM).[14] However, the rapid oxidation of the Al top electrode

* Address correspondence to chunwei@ntu.edu.tw.

Received for review May 26, 2011 and accepted July 12, 2011.

Published online July 12, 2011
10.1021/nn201940j

usually causes instability and degradation of device performance. An alternative type of so-called inverted device architecture, where the anode and cathode are reversed, was found to overcome this problem by using an air-stable, high-workfunction metal such as Ag or Au as the top electrode.[15] Here, we will utilize the laminated graphene electrode to replace the top metal electrode for fabricating a semitransparent inverted polymer solar cell with a device structure consisting of ITO/ZnO/P3HT:PCBM/graphene oxide (GO)/graphene top electrode, as shown in Figure 1. For the fabrication of an inverted-type device, a thin ZnO layer was first deposited on top of the ITO electrode to act as the electron-selective layer to block hole transporting.[16] The P3HT:PCBM hybrid photoactive layer was deposited on top of the thin ZnO layer with a typical thickness of 250 nm. In our previous work, we demonstrated that graphene oxide (GO), which is a graphene sheet functionalized with oxygen groups and containing a large fraction of sp^3-hybridized carbon atoms, is a promising candidate for replacing the conventional PEDOT:PSS to act as a hole transporting layer.[17] The GO thin film with an average thickness of ~2 nm was thus deposited from neutral solutions on top of the P3HT:PCBM hybrid photoactive layer (step A, Figure 2a). The thin GO film consists of many individual GO flakes with lateral dimensions ranging from 5 to 10 μm.[17,18] The device consisting of the structure ITO/ZnO/P3HT:PCBM/GO was thus kept in the glovebox for further deposition of the top electrode.

For the preparation of the graphene top electrode, we synthesized a graphene film grown on copper foil using chemical vapor deposition (CVD) processes.[19] After growth, the surface of the graphene film with copper foil was attached to thermal release tape (Nitto Denko). Then, the copper foil was etched by immersing the sample into an iron nitrate solution (0.4 g/mL) (step B, Figure 2a). The graphene film with thermal release tape was rinsed with deionized water to remove the residual etchant and then dried by N_2 flow. Because a single layer of graphene does not have sufficiently high sheet conductivity, multilayer stacking of the graphene films is usually required to obtain higher sheet conductance. In this work, we modified the roll-to-roll production method that was reported by S. Bae *et al.*[20] to transfer the graphene film. Instead of using thermal release tape while transferring each layer of graphene, we used only the first layer of graphene with thermal release tape to be attached onto the second layer of graphene on copper foil (step C, Figure 2a), which was subsequently rolled by the roller. After etching the copper foil, the two-layer graphene film with thermal release tape was further attached to another graphene on copper foil to obtain a three-layer graphene, which can minimize the possible contamination from a residual organic impurity between the graphene layers during film transfer.[11] Here, we used a maximum of four layers

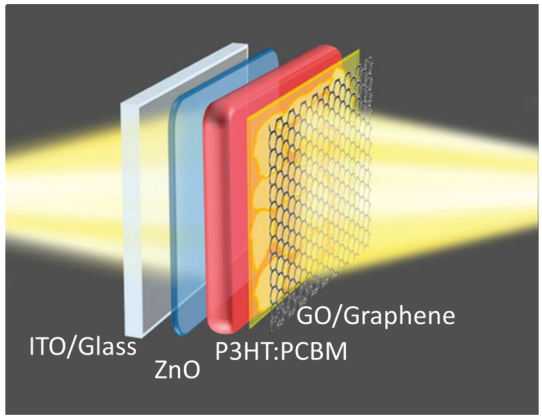

Figure 1. Semitransparent inverted polymer solar cell with a structure of ITO/ZnO/P3HT:PCBM/graphene oxide (GO)/graphene top electrode.

of graphene with one thermal release tape during each transfer to other substrates or devices, followed by the removal of the top thermal release tape. The procedures were repeated to obtain a graphene electrode with optimal conductance and transparency. The crystalline quality of the graphene films consisting of different layers as transferred onto the glass substrate was first analyzed by Raman spectroscopy, as shown in Figure 2b. The G peak (~1583 cm^{-1}) of the graphene Raman spectrum corresponds to the E_{2g} phonon at the Brillouin zone center, whereas the D peak (~1320 cm^{-1}) is caused by the breathing mode of sp^2 atoms and is activated by the existence of defects.[21] Because the width and shape of a 2D peak (~2642 cm^{-1}) are highly related to the layer number and stacking order, no obvious change in the intensity ratios of I_{2D}/I_G suggests that the sequentially transferred graphene layers were of random stacking order.[22] In addition, a low-defect-related D-band peak was observed, indicating that the as-grown graphene films are of high crystalline quality. The transmittance of the graphene film is reduced about 2−3% as each layer of graphene was added, as shown in Figure 2c, and the sheet resistance of the graphene film decreases with increasing number of layers, as shown in Figure 2d. For the deposition of the top graphene electrode, the graphene film with thermal release tape was thus placed on top of the ITO/ZnO/P3HT:PCBM/GO device followed by the removal process (Figure 2a, step D). In the fabrication of polymer solar cells, thermal annealing is a widely used approach for improving the power conversion efficiency of devices by controlling the nanoscaled morphology of a P3HT:PCBM blend.[14] The removal of thermal release tape from the graphene film was thus simultaneously conducted during thermal annealing treatment, where the entire device of ITO/ZnO/P3HT:PCBM/GO/graphene film with thermal release tape was heated on a hot plate at 120 °C, and the total annealing/releasing time of the device was controlled to be 10 min. All simultaneous thermal annealing/releasing procedures were conducted in the

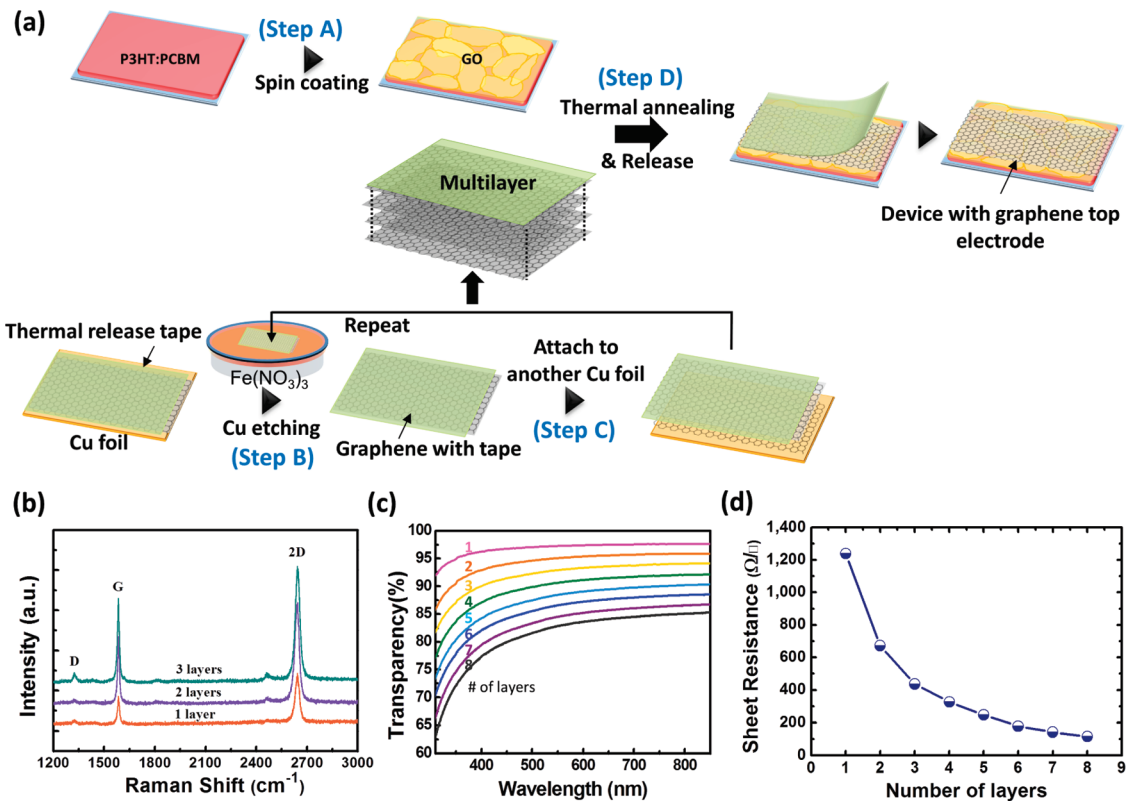

Figure 2. (a) Fabrication of the ITO/ZnO/P3HT:PCBM/GO device before depositing the top electrode (step A). Top lamination processes of graphene electrodes by the graphene film transferring (steps B, C) and thermal annealing/releasing processes (step D). (b) Raman spectroscopy of the graphene films consisting of one, two, and three layers on a glass substrate. (c and d) Transmittance and sheet resistance of the graphene films on a glass substrate consisting of various numbers of layers.

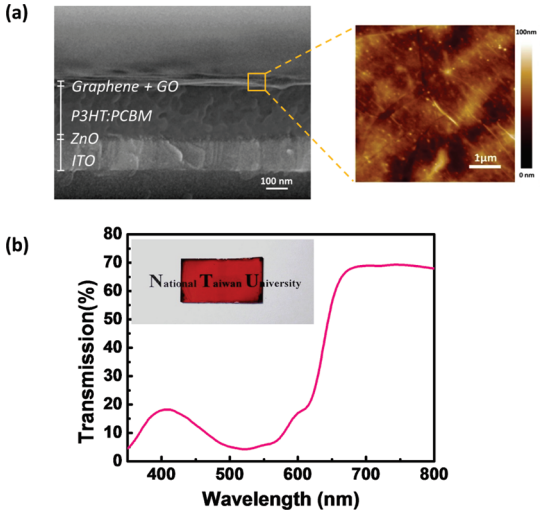

Figure 3. (a) Cross-sectional SEM image and (b) morphological AFM image of the device structure of the ITO/ZnO/P3HT:PCBM/GO/graphene top electrode (six layers). (c) Transmittance of this semitransparent polymer solar cell. A picture of the semitransparent device is shown in the inset.

glovebox. The cross-sectional SEM image of the semitransparent solar cell consisting of a device structure of ITO/ZnO/P3HT:PCBM/GO/graphene top electrode (six layers) is shown in Figure 3a, and the morphological image of the top laminated graphene electrode revealed by atomic force microscopy (AFM) is also shown in Figure 3b. The semitransparent polymer solar cell with both cathode (ITO) and anode (graphene) being transparent is shown in the inset of Figure 3c. The area of each device is about 10 mm^2. The transmittance spectrum of the semitransparent solar cell is shown in Figure 3b, and a high transparency with wavelengths beyond 700 nm was obtained where P3HT/PCBM has no absorption, which makes the graphene-based semitransparent solar cells a promising candidate for the applications of power-generated windows or multijunction solar cells.

Figure 4a,b plots the current−voltage characteristics of the semitransparent polymer solar cells consisting of the top laminated graphene electrodes with various number of graphene layers with light shining from the ITO side or the graphene side, respectively (A.M. 1.5 illumination, 100 mW cm^{-2}). For comparison, the device performance of a standard opaque inverted device consisting of the Ag top electrode with a structure of ITO/ZnO/P3HT:PCBM/GO/Ag is also shown, exhibiting a short circuit current (J_{sc}) of 11.5 mA/cm^2, an open circuit voltage (V_{oc}) of 0.52 V, and a fill factor (FF) of 0.55, yielding a power conversion efficiency of 3.30%. Table 1 summarizes the photovoltaic performances of these devices. All the semitransparent devices show a similar V_{oc} of 0.54 V, regardless of whether the light was

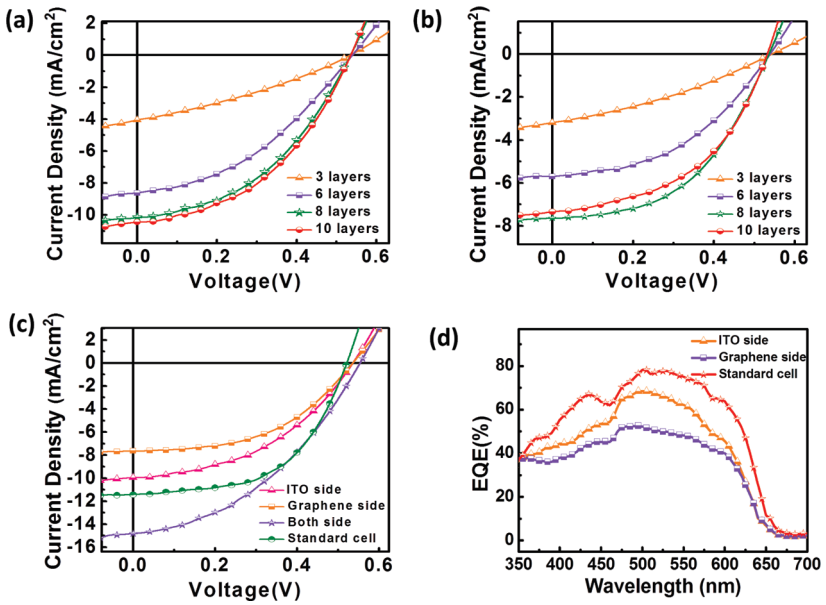

Figure 4. (a and b) Current−voltage characteristics of the semitransparent polymer solar cells consisting of various number of top graphene layers with light shining from the ITO side or the graphene side, respectively (A.M. 1.5 illumination, 100 mW/cm^2). (c and d) Device performances and EQEs of the standard cell and semitransparent cell consisting of eight layers of graphene as illuminated from the ITO side and the graphene side. The device performance of the semitransparent cell under simultaneous illumination from both sides is also shown in (c).

TABLE 1. Summary of the Device Performances of the Semitransparent Polymer Solar Cells under Illumination (A.M. 1.5, 100 mW/cm^2) from the ITO Side and the Graphene Side (parentheses) and the Device Performance of the Reference Standard Opaque Device

ITO (graphene)	V_{oc} (V)	J_{sc} (mA/cm^2)	FF	PCE (%)
10 layers	0.54(0.54)	10.50(7.35)	0.44(0.47)	2.50(1.88)
8 layers	0.54(0.54)	10.10(7.70)	0.44(0.49)	2.40(2.04)
6 layers	0.54(0.54)	8.62(5.71)	0.39(0.44)	1.82(1.36)
3 layers	0.54(0.54)	4.05(3.19)	0.32(0.33)	0.69(0.57)
standard cell (Ag electrode)	0.52	11.5	0.55	3.30

incident from the ITO or graphene side. The semitransparent devices through illumination from the ITO side exhibit larger J_{sc} and higher PCEs compared to devices illuminated from the graphene side. As illuminated from the ITO side, the semitransparent device achieves a best PCE of 2.50% when the device consists of a top electrode with 10 layers of graphene, corresponding to 76% of that of the standard opaque cell. Further increase in the layer number of the graphene electrode does not cause a remarkable change in the PCE as illuminated from the ITO side. By contrast, while illuminated from the graphene side, the semitransparent device consisting of eight layers of graphene exhibits an optimal PCE of 2.04%, which is approximately 62% of that of the standard cell. Figure 4c shows the current−voltage characteristics of the standard cell and semitransparent cell consisting of eight layers of graphene as the top electrode under illumination from the ITO side or the graphene side, respectively. The corresponding external quantum efficiencies (EQEs) of these devices are also shown in Figure 4d. Interestingly, when both sides of the semitransparent device were simultaneously illuminated under the same light source (100 mW cm^{-2}) at an incident angle of 45° to both electrodes of the device using a reflected mirror set (Supporting Information), the J_{sc} and V_{oc} of the device were increased to 14.8 mA cm^{-2} and 0.55 V, respectively, while the FF slightly decreased to a value of 0.41, suggesting the potential application of the graphene-based semitransparent solar cells in the bifacial photovoltaic devices.[23]

Figure 5a exhibits the dark current−voltage characteristics of the semitransparent (eight layers of graphene) and standard devices on a semilogarithmic scale. Although the semitransparent solar cell with the graphene top electrode exhibits good diode behavior with a rectification ratio of approximately 3 orders in magnitude at biases ±1 V, the device is much more resistive in the forward bias region with a higher serial resistance (8.62 Ω cm^2) compared to that of the standard cell (2.33 Ω cm^2). The higher serial resistance of the semitransparent device is mainly attributed to a larger sheet resistance of the graphene electrode and also a larger contact resistance between the polymer blend and the anode. In addition, the asymmetric photovoltaic performances of the semitransparent device as illuminated from two respective sides with a larger difference in J_{sc} (~30%) accompanied by different shapes of EQE spectra were also observed. To further clarify this effect, we performed the transient photovoltage (TPV) measurement to probe the photocarrier recombination behaviors of the semitransparent

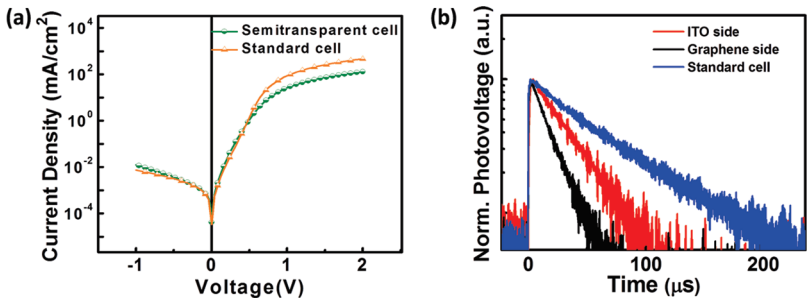

Figure 5. (a) Dark current−voltage characteristics of the standard cell and the semitransparent cell (eight layers) on a semilogarithmic scale. (b) Transient photovoltage (TPV) decay curves of the standard cell and the semitransparent cell measured from two different illuminating directions. Devices were illuminated by white light with a power intensity of 50 mW/cm^2.

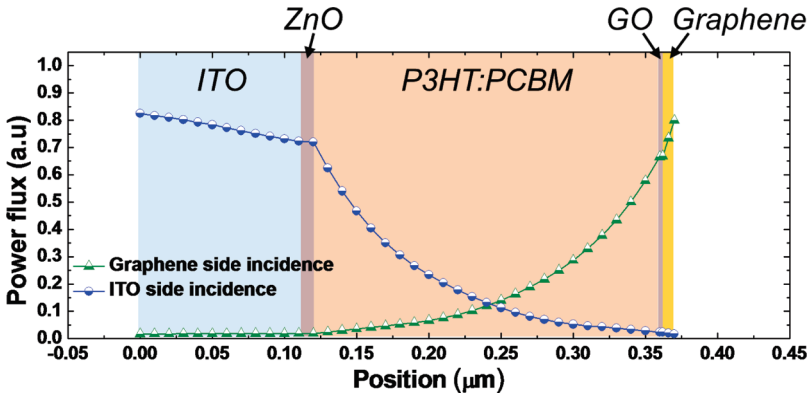

Figure 6. Power flux distributions of incident light inside the semitransparent device as illuminated from two respective sides using the 3D-FDTD simulation.

solar cell with different illuminating directions, as shown in Figure 5b. The details of the TPV measurement have been described elsewhere.[24] Briefly, devices were illuminated by white light and operated at the steady-state V_{oc} condition. A small perturbed short laser pulse was used to generate extra photocarriers having a recombination lifetime of τ, as indicated by the transient decay of the photovoltage. The recombination rate k_{rec} of the device is therefore proportional to $1/\tau$. The recombination lifetime τ in the semitransparent device was found to be longer as illuminated from the ITO side (35.7 μs) than that from the graphene side (18.6 μs). Because the same device was used for two respective measurements, the lower recombination rate of the device illuminated from the ITO side is mainly attributed to the higher carrier collection efficiency as a result of lower sheet resistance of ITO. The standard opaque cell exhibits an even longer recombination time (66.3 μs) than the semitransparent device, indicating a more efficient carrier collection.

Finally, we examined the power flux distribution of incident light inside the semitransparent device as illuminated from two respective sides using the three-dimensional finite difference time domain (3D-FDTD) simulation (Fullwave, RSoft Design Group). For comparison, the transmittances of the ITO/glass and graphene/graphene oxide electrodes within the whole solar light spectrum are shown in the Supporting Information. The FDTD method discretized Maxwell's equations by the central difference in time and space and numerically solved the equations to provide insight into the near-field optical behaviors. The quantity of power flux gives the time-average magnitude of the Poynting vector, representing the energy flow in the near field. The simulated structure was based on the multilayer device model of ITO(150 nm)/ZnO(10 nm)/P3HT:PCBM(250 nm)/GO(2 nm)/graphene(8 nm), and all the simulated optical parameters of refractive indices were obtained from the values reported in the literature.[25−29] The details of the simulation parameters are also included in the Supporting Information. The incident light with a wavelength of 550 nm at which P3HT has a larger absorption coefficient was used in the simulation. The thin graphene electrode has about 15% light absorption, and the light-harvesting efficiency of the P3HT:PCBM active layer is slightly lower (~5%) as illuminated from the graphene side than that as illuminated from the ITO side, as shown in Figure 6. Because the active layer of the semitransparent device is comparably thick (~250 nm), a higher density of excited carriers is close to the incident electrodes, regardless of whether the light was incident from the ITO or graphene side.

The power flux in the middle of the active layer was reduced to about 10%, and very low transmitted power reached the other side. Since the concentrations of photogenerated carriers of electrons and holes decrease exponentially with absorption depths, the device performance is expected to depend strongly on the collection efficiency of the incident electrode, giving asymmetric photovoltaic behavior of the graphene-based semitransparent solar cell. The effect of the asymmetric photovoltaic performance on the incident electrodes is expected to be stronger when the incident light has a shorter penetration depth. This can explain the larger EQE difference under the illuminations from the two different sides ($\Delta EQE(\lambda)$) at the wavelengths with higher absorption of the active layer, as shown in Figure 4d.

In this work, we demonstrate a semitransparent organic photovoltaic device that uses a top laminated graphene electrode on an inverted-type polymer solar cell using a simultaneous thermal releasing/annealing technique. The deposition of the top graphene electrode is fully compatible with the roll-to-roll manufacturing in the future market integration of low-cost plastic solar cells. Further optimization in the conductivity of the graphene electrode by chemical doping or defect reduction is the next step for improving the performance of graphene-based semitransparent solar cells.

EXPERIMENTAL SECTION

Preparation of Graphene and Graphene Oxide. A polycrystalline Cu foil, purchased from Nilaco, was placed on a hot wall furnace consisting of a 1.5 in. fused silica tube. The furnace was then heated to 950 °C. Typically, a reduction process was conducted in H_2 flow for ~30 min prior to the introduction of CH_4. With H_2 flow, CH_4 was then introduced for graphene growth with a flow rate of 50 and 10 sccm for H_2. After a growth time of 15 min, CH_4 was then shut off and the system was cooled in a H_2 or Ar flow to reach room temperature. The whole procedure was conducted at low pressure (typically ~500 mTorr during the growth stage). Graphene oxide was obtained from purified natural graphite powder (SP-1, Bay Carbon) using the modified Hummers method as reported in ref 18. As-synthesized GO was dispersed in deionized water with a concentration of 8 mg/mL and then diluted by IPA (isopropyl alcohol) with a 1:1 volume ratio for deposition of GO thin films.

Device Fabrication. A semitransparent solar cell was fabricated with a standard inverted structure replacing the PEDOT:PSS hole transporting layer by GO and the top metal electrode by the laminated graphene film. The resulting device structure was ITO/ZnO/P3HT:PCBM/GO/graphene. ITO substrates were etched and cleaned with solvents. The substrates were further treated with oxygen plasma for 5 min before the deposition of the ZnO layer, which was prepared by the sol−gel method, acting as an electron-selective layer. Zinc acetate dihydrate ($Zn(CH_3COO)_2 \cdot 2H_2O$) was dissolved in a mixture of 1-propanol ($CH_3CH_2CH_2OH$) and ethanolamine ($NH_2CH_2CH_2OH$) solution under stirring at 60 °C for 1 h for the hydrolysis reaction. The molar ratio of ethanolamine to zinc acetate was maintained at 1, and the concentration of zinc acetate was 0.02 M. The as-prepared ZnO precursor was then spin-coated on ITO substrates and air annealed at 200 °C for 1 h. The photoactive layer was deposited on top of the ZnO layer by spin coating using a 1:1 weight ratio blend consisting of P3HT (Rieke Metal) and PCBM (Nano-C) dissolved in chlorobenzene (20 mg mL^{-1}) followed by the deposition of GO. Finally the devices were completed with laminated graphene as a top electrode and thermal evaporation of Ag (100 nm) for a standard cell.

Materials and Device Characterizations. UV−visible absorption spectra were obtained using a Jasco V-570 UV/vis/NIR spectrophotometer. The Raman measurement was conducted using a 633 nm laser excitation. Current−voltage characteristics (Keithley 2410 source meter) were obtained by using a solar simulator (Newport Inc.) with the A.M. 1.5 filter under an irradiation intensity of 100 mW/cm^2. For the transient photovoltage decay measurement, the devices were measured at open-circuit conditions under illumination from the solar simulator with adjustable intensities. A small perturbation generated by a pulse from a frequency-doubled Nd:YAG pulsed laser (λ = 532 nm, repetition rate = 10 Hz, duration ~5 ns) was used. The transient decay signals were recorded by a digital oscilloscope (Tetronix TDS5052B).

Acknowledgment. This work is supported by National Science Council, Taiwan, for the project "Core facilities of novel graphene based materials" (Project Nos. NSC 98-2119-M-002-020- and 99-2119-M-002-012-).

Supporting Information Available: Description of the setup for bifacial solar cell measurement, transmittance of ITO/glass and graphene/GO electrodes, and optical simulations. This material is available free of charge *via* the Internet at http://pubs.acs.org.

REFERENCES AND NOTES

1. Granström, M.; Petritsch, K.; Arias, A. C.; Lux, A.; Andersson, M. R.; Friend, R. H. Laminated Fabrication of Polymeric Photovoltaic Diodes. *Nature* **1998**, *395*, 257–260.
2. Brabec, C. J.; Sariciftci, N. S.; Hummelen, J. C. Plastic Solar Cells. *Adv. Funct. Mater.* **2001**, *11*, 15–26.
3. Shaheen, S. E.; Ginley, D. S.; Jabbour, G. E. Organic-Based Photovoltaics: Toward Low-Cost Power Generation. *MRS Bull.* **2005**, *30*, 10–15.
4. Koeppe, R.; Hoeglinger, D.; Troshin, P. A.; Lyubovskaya, R. N.; Razumov, V. F.; Sariciftci, N. S. Organic Solar Cells with Semitransparent Metal Back Contacts for Power Window Applications. *ChemSusChem* **2009**, *2*, 309–313.
5. Xia, X.; Wang, S.; Jia, Y.; Bian, Z.; Wu, D.; Zhang, L.; Cao, A.; Huang, C. Infrared-Transparent Polymer Solar Cells. *J. Mater. Chem.* **2010**, *20*, 8478–8482.
6. Huang, J.; Li, G.; Yang, Y. A Semi-Transparent Plastic Solar Cell Fabricated by a Lamination Process. *Adv. Mater.* **2008**, *20*, 415–419.
7. Zhou, Y.; Cheun, H.; Choi, S.; Potscavage, W. J., Jr.; Fuentes-Hernandez, C.; Kippelen, B. Indium Tin Oxide-Free and Metal-Free Semitransparent Organic Solar Cells. *Appl. Phys. Lett.* **2010**, *97*, 153304.
8. Lee, J. Y.; Connor, S. T.; Cui, Y.; Peumans, P. Solution-Processed Metal Nanowire Mesh Transparent Electrodes. *Nano Lett.* **2008**, *8*, 689–692.
9. Zhang, Y.; Tan, Y. W.; Stormer, H. L.; Kim, P. Experimental Observation of the Quantum Hall Effect and Berry's Phase in Graphene. *Nature* **2005**, *438*, 201–204.
10. Nair, R. R.; Blake, P.; Grigorenko, A. N.; Novoselov, K. S.; Booth, T. J.; Stauber, T.; Peres, N. M. R.; Geim, A. K. Fine Structure Constant Defines Visual Transparency of Graphene. *Science* **2008**, *320*, 1308.
11. Wang, Y.; Tong, S. W.; Xu, X. F.; Özyilmaz, B.; Loh, K. P. Graphene: Interface Engineering of Layer-by-Layer

Stacked Graphene Anodes for High-Performance Organic Solar Cells. *Adv. Mater.* **2011**, *23*, 1514–1518.
12. Park, H.; Rowehl, J. A.; Kim, K. K.; Bulovic, V.; Kong, J. Doped Graphene Electrodes for Organic Solar Cells. *Nanotechnology* **2010**, *21*, 505204.
13. Chang, H.; Wang, G.; Yang, A.; Tao, X.; Liu, X.; Shen, Y.; Zheng, Z. A Transparent, Flexible, Low-Temperature, and Solution-Processible Graphene Composite Electrode. *Adv. Funct. Mater.* **2010**, *20*, 2893–2902.
14. Li, G.; Shrotriya, V.; Huang, J.; Yao, Y.; Moriarty, T.; Emery, K.; Yang, Y. High-Efficiency Solution Processable Polymer Photovoltaic Cells by Self-Organization of Polymer Blends. *Nat. Mater.* **2005**, *4*, 864–868.
15. Glatthaar, M.; Niggemann, M.; Zimmermann, B.; Lewer, P.; Riede, M.; Hinsch, A.; Luther, J. Organic Solar Cells Using Inverted Layer Sequence. *Thin Solid Films* **2005**, *491*, 298–300.
16. White, M. S.; Olson, D. C.; Shaheen, S. E.; Kopidakis, N.; Ginley, D. S. Inverted Bulk-Heterojunction Organic Photovoltaic Device Using a Solution-Derived ZnO Underlayer. *Appl. Phys. Lett.* **2006**, *89*, 143517.
17. Li, S. S.; Tu, K. H.; Lin, C. C.; Chen, C. W.; Chhowalla, M. Solution-Processable Graphene Oxide as an Efficient Hole Transport Layer in Polymer Solar Cells. *ACS Nano* **2010**, *4*, 3169–3174.
18. Eda, G.; Fanchini, G.; Chhowalla, M. Large-Area Ultrathin Films of Reduced Graphene Oxide as a Transparent and Flexible Electronic Material. *Nat. Nanotechnol.* **2008**, *3*, 270–274.
19. Hwang, J. Y.; Kuo, C. C.; Chen, L. C.; Chen, K. H. Correlating Defect Density with Carrier Mobility in Large-Scaled Graphene Films: Raman Spectral Signatures for the Estimation of Defect Density. *Nanotechnology* **2010**, *21*, 465705.
20. Bae, S.; Kim, H.; Lee, Y.; Xu, X.; Park, J. S.; Zheng, Y.; Balakrishnan, J.; Lei, T.; Kim, H. R.; Song, Y. I.; *et al*. Roll-to-Roll Production of 30-Inch Graphene Films for Transparent Electrodes. *Nat. Nanotechnol.* **2010**, *5*, 574–578.
21. Ferrari, A. C. Raman Spectroscopy of Graphene and Graphite: Disorder, Electron−Phonon Coupling, Doping and Nonadiabatic Effects. *Solid State Commun.* **2007**, *143*, 47–57.
22. Ferrari, A. C.; Meyer, J. C.; Scardaci, V.; Casiraghi, C.; Lazzeri, M.; Mauri, F.; Piscanec, S.; Jiang, D.; Novoselov, K. S.; Roth, S.; *et al*. Raman Spectrum of Graphene and Graphene Layers. *Phys. Rev. Lett.* **2006**, *97*, 187401.
23. Hezel, R. Novel Applications of Bifacial Solar Cells. *Prog. Photovoltaics Res. Appl.* **2003**, *11*, 549–556.
24. Lin, Y. Y.; Chu, T. H.; Li, S. S.; Chuang, C. H.; Chang, C. H.; Su, W. F.; Chang, C. P.; Chu, M. W.; Chen, C. W. Interfacial Nanostructuring on the Performance of Polymer/TiO_2 Nanorod Bulk Heterojunction Solar Cells. *J. Am. Chem. Soc.* **2009**, *131*, 3644–3649.
25. Ni, Z. H.; Wang, H. M.; Kasim, J.; Fan, H. M.; Yu, T.; Wu, Y. H.; Feng, Y. P.; Shen, Z. X. Graphene Thickness Determination Using Reflection and Contrast Spectroscopy. *Nano Lett.* **2007**, *7*, 2758–2763.
26. Jung, I.; Vaupel, M.; Pelton, M.; Piner, R.; Dikin, D. A.; Stankovich, S.; An, J.; Ruoff, R. S. Characterization of Thermally Reduced Graphene Oxide by Imaging Ellipsometry. *J. Phys. Chem. C* **2008**, *112*, 8499–8506.
27. Synowicki, R. A. Spectroscopic Ellipsometry Characterization of Indium Tin Oxide Film Microstructure and Optical Constants. *Thin Solid Films* **1998**, *313−314*, 394–397.
28. Bass, M. *Handbook of Optics*, 2nd ed.; McGraw-Hill: New York, USA, 1994, Vol. 2.
29. Chuang, S. Y.; Chen, H. L; Lee, W. H.; Huang, Y. C.; Su, W. F.; Jen, W. M.; Chen, C. W. Regioregularity Effects in the Chain Orientation and Optical Anisotropy of Composite Polymer/Fullerene Films for High-Efficiency, Large-Area Organic Solar Cells. *J. Mater. Chem.* **2009**, *19*, 5554–5560.